Scripta Materialia 138 (2017) 39–43

Contents lists available at ScienceDirect

Scripta Materialia

journal homepage: www.elsevier.com/locate/scriptamat

Regular Article

Direct observation of precipitation along twin boundaries and dissolution in a magnesium alloy annealing at high temperature

Dikai Guan, John Nutter, Joanne Sharp, Junheng Gao, W. Mark Rainforth *

Department of Materials Science and Engineering, The University of Sheffield, Sheffield S1 3JD, UK

ARTICLE INFO

Article history:
Received 14 March 2017
Received in revised form 8 May 2017
Accepted 12 May 2017
Available online xxxx

Keywords:
Magnesium alloy
Twinning
Annealing
Precipitation
Recrystallization

ABSTRACT

Precipitation along twin boundaries and dissolution in a cold-rolled Mg-Y-Nd alloy was directly observed for the first time during annealing at 490 °C. Precipitation occurred concurrently with recrystallization and the combined effect of precipitation and solute segregated to twin boundaries modified the recrystallization behaviour. Precipitates later dissolved into the matrix at the point where full recrystallization was nearly complete. The precipitates and higher solute concentration along original twin boundaries hindered grain growth of newly formed recrystallized grains. Even where twin boundaries had been consumed by recrystallization, the size of recrystallized grains were still controlled by the pre-existing twin boundaries.

It is often reported that segregation and precipitation along grain boundaries (GBs) can minimise the local stored energy induced by deformation [1–5]. Grain growth kinetics are also altered due to solute drag or by particle pinning effects [6,7]. Segregation along fully coherent twin boundaries was first reported by Nie et al. [8] who observed periodic segregation of Gd and Zn atoms along twin boundaries when the sample was cold compressed and annealed at 150 °C. The solute drag restricted the movement of twin boundaries and improved the compressive strength. Later, Somekowa et al. [9] reported that segregation along twin boundaries increased hardness but degraded damping capacity in a cold compressed sample after annealing at 250 °C. Basha et al. [10] even found Zn segregation along twin boundaries during cold compression without any heat treatment. Precipitation along twin boundaries has been reported by Ye et al. [11] who found this phenomenon in a pre-strained Mg alloy after ageing at 200 °C. However, in all aforementioned reports, the segregation or precipitation along twin boundaries was only observed at low annealing temperatures, where no recrystallization occurred.

Recrystallization leading to a reduction in basal texture intensity of wrought Mg alloys has been the focus of considerable attention [12–16], since weakening the basal texture can significantly reduce anisotropic mechanical properties and improve the formability of Mg alloys. In deformed Mg alloys, grain and twin boundaries are effective sites for static recrystallization. However, recrystallization temperatures are usually higher than the temperatures used for ageing. The question therefore arises: does this segregation or precipitation happen at high temperatures? If it does, does the segregation and precipitation remain throughout the whole static recrystallization process when the original twin boundaries have disappeared due to recrystallization? How does the segregation and precipitation interact with the recrystallized grains?

To address these issues, *in-situ* TEM, *quasi-in-situ* EBSD and SEM were employed to track the entire static recrystallization process during annealing at 490 °C. We observed, for the first time, the precipitation process on twin boundaries concurrent with recrystallization and dissolution of the precipitates when full recrystallization had nearly finished.

The as-received material was a commercial WE43 alloy supplied by Magnesium Elektron as extruded T5 bar with the chemical composition listed in Table 1 of our previous study [17]. Solid solution treatments were undertaken under a continuous argon flow at 525 °C for 10 min and 1 h, followed by cold water quenching. The corresponding samples were designated as SST10M and SST1H, respectively. Subsequently, the samples was cold rolled by a reduction in thickness of 20% in one pass, with the samples designated SST10MCR and SST1HCR. Recrystallization rate is dependent on original grain size; a fine-grained sample usually recrystallizes more quickly than a coarse-grained sample. Therefore, we chose a short solid solution treatment in order to provide a fine-grained material that would recrystallize quickly, allowing us to observe precipitation and precipitation dissolution in an acceptable experimental time by using *in-situ* TEM. In contrast, a coarse-grained SST1HCR was used for quasi-*in-situ* EBSD experiments as we needed to slow down recrystallization rate to track the microstructure evolution in a large sample area.

EBSD was performed using a FEI Nano Nova 450 field emission gun SEM fitted with Oxford Instruments HKL NordlysMax^3 EBSD detector. The EBSD scans were taken after cold rolling and after 300 s, 720 s,

* Corresponding author.
E-mail address: m.rainforth@sheffield.ac.uk (W. Mark Rainforth).

http://dx.doi.org/10.1016/j.scriptamat.2017.05.015

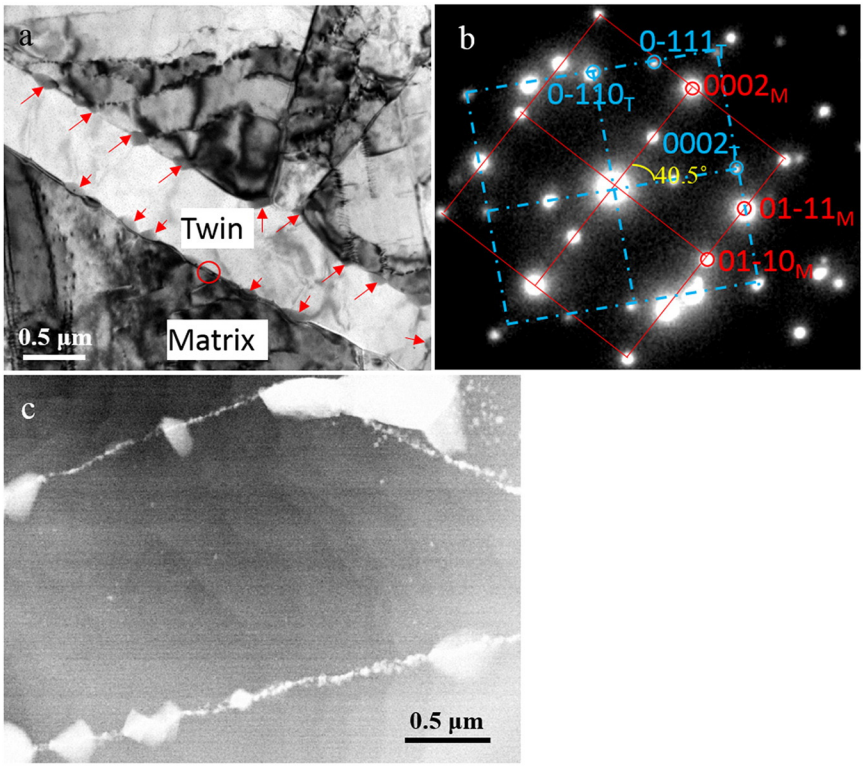

Fig. 1. (a) TEM BF image, (b) corresponding SADP image from interface between twin and matrix (see red circle shown in (a)) and (c) STEM HAADF image of sample SST10MCR after annealing at 490 °C for 5 min. (For interpretation of the references to colour in this figure, the reader is referred to the web version of this article.)

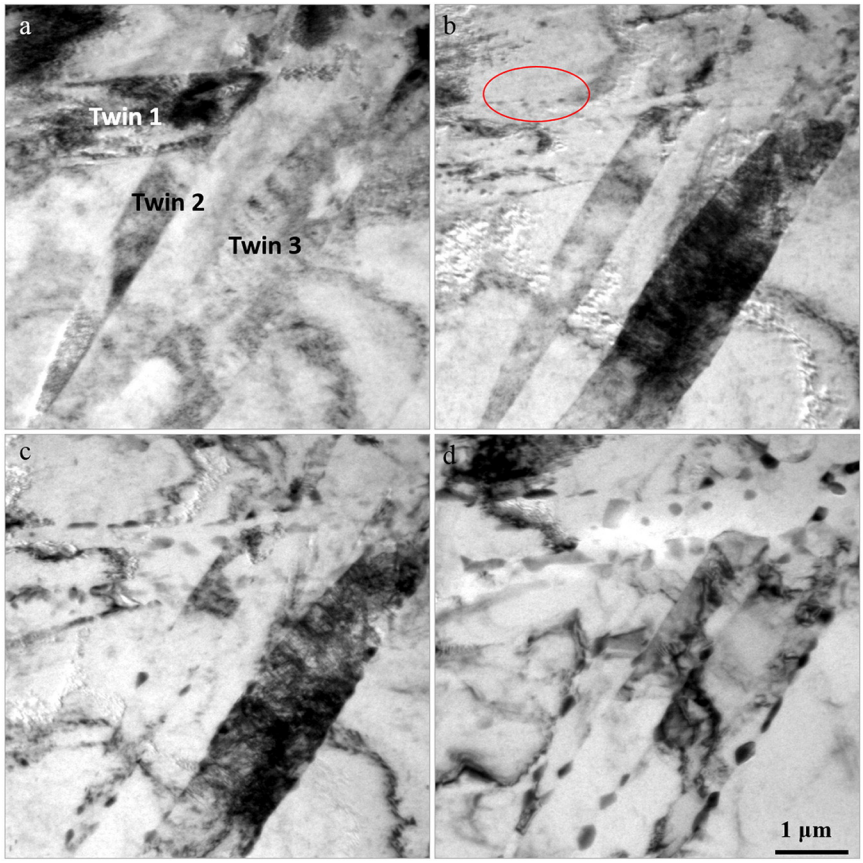

Fig. 2. *In-situ* TEM BF images of sample SST10MCR: (a) as-cold rolled, (b) after heating 362 s when the temperature was up to 350 °C, (c) after heating 471 s when the temperature was up to 400 °C, and (d) after heating 793 s and the temperature held at 400 °C for 322 s. All the temperatures were controlled by hot stage heating unit instead of actual values of TEM sample temperature.

1260s, 9780 s, 14,520 s, and 20,460 s annealing at 490 °C. The EBSD scanning area was precisely rescanned after each annealing at 490 °C by *quasi-in-situ* method, and the experimental details can be found in [17]. Observation along the Z direction in CS0 (sample primary) instead of CS1 (acquisition surface) coordinate system was applied to all the EBSD inverse pole figure (IPF) legends. Thin foil TEM samples from cold-rolled and annealed samples were initially mechanically ground to 100 μm and thinned by twin-jet thinning, followed by a low angle ion milling using a Gatan PIPS II machine to clean the surface before TEM. An FEI Tecnai T20 microscope operated at 200 kV was employed for microstructural observations. Scanning TEM (STEM) high angle annular dark field imaging (HAADF) images were taken using a JEOL 2010F microscope. A JEOL 3010 microscope was used to record the microstructure evolution during heating process by using a GATAN model 628 heating holder.

The microstructure of the cold rolled SST10MCR and SST1HCR comprised profuse deformation twins within the matrix. The solution treatment had dissolved the vast majority of precipitates, but a few sparsely distributed residual intermetallic particles remained. Fig. S1 in Supplementary file provides the SEM and corresponding EBSD images. After annealing at 490 °C for several minutes, small precipitates started to appear along original grain and twin boundaries that were hitherto free from precipitates. Fig. S2 shows a backscattered SEM image of sample SST10MCR after 5 min annealing, while Fig. 1(a) shows a representative TEM bright field (BF) image and Fig. 1(b) is the corresponding selected area diffraction pattern (SADP) from the interface between twin and matrix (see red circle). The zone axis was determined to be $\langle 2\bar{1}\ \bar{1}0\rangle$, and therefore the disorientation between twin area and the matrix area is $\langle 2\bar{1}\ \bar{1}0\rangle$ 40.5°. This disorientation is within experimental error of the theoretical double twin $\{10\bar{1}1\}$–$\{10\bar{1}2\}$ relationship $\langle 2\bar{1}\ \bar{1}0\rangle$ 38° [18]. In addition, precipitates can be seen distributed discontinuously along twin boundaries, as indicated by red arrows in Fig. 1(a). Fig. 1(c) gives a STEM-HAADF image of sample SST10MCR after annealing for 5 min. Precipitates around several hundred nanometers were present, along with smaller precipitates and segregation along the twin boundaries. These particles were not observed in the matrix or within the twins. The bright contrast in Fig. 1(c) indicated that the precipitates and segregation had a higher average atomic number than the matrix. Fig. S3 provides an EDX line scan of a twin boundary from SST10MCR after annealing 1200s. Fig. S3(b) clearly shows the main alloying elements Y, Nd and Zr enriched along the twin boundaries.

To identify the origin of the precipitates, *in-situ* TEM heating experiments were employed. Fig. 2 shows a sequence of images of sample SST10MCR during heating in the TEM. The heating curve can be found in Fig. S4. Fig. 2(a) clearly shows there were three main twins in the investigated area (labelled in Fig. 2(a)) before heating started. The twin boundaries and matrix were largely free from precipitates after cold rolling. After heating the sample for 362 s when the temperature of TEM holder control unit reached 350 °C, small precipitates formed discontinuously along twin 1 boundary (as shown in red oval). It should be noted that the temperature of the hot stage control unit was not the same as the specimen temperature (due to thermal losses from the specimen), which was estimated to be about 100 °C lower than the actual temperature of sample. When the nominal temperature was increased to 400 °C for 471 s, all the twin boundaries became decorated by precipitates, Fig. 2(c). However, no precipitates were observed within matrix or in the twin interior. Fig. 2 (d) shows the same area after holding at 400 °C for another 332 s. The precipitates on the twin boundaries coarsened, but

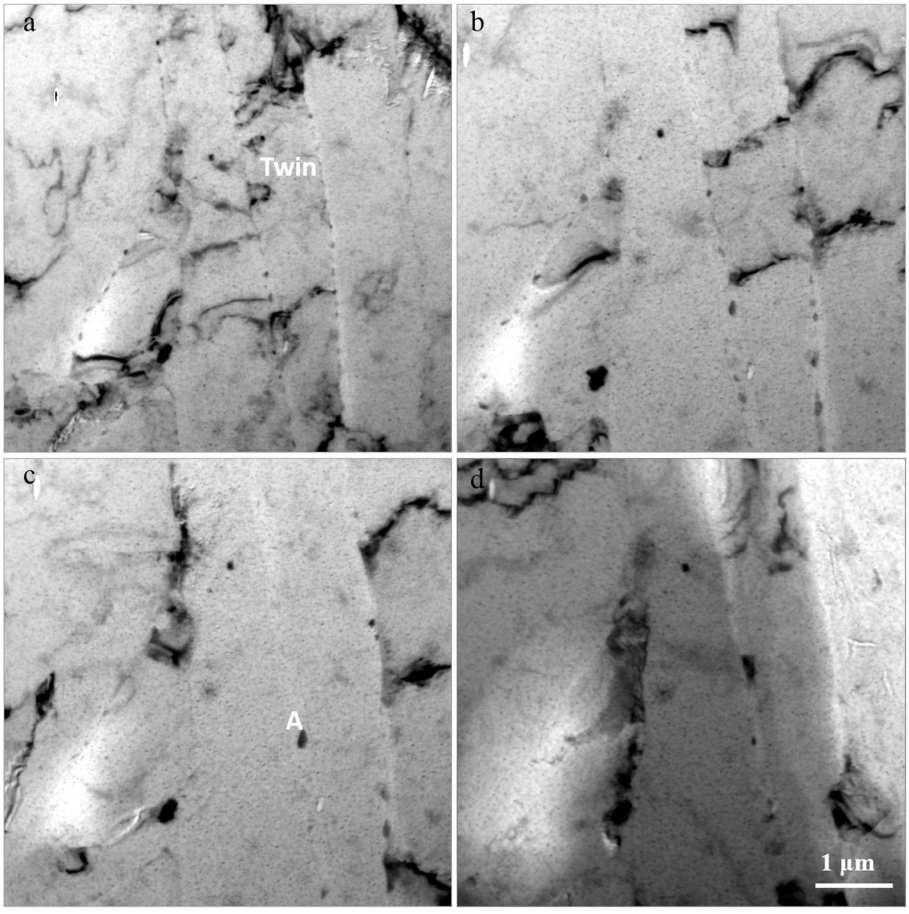

Fig. 3. *In-situ* TEM BF images of sample SST10MCR: (a) after heating up to 450 °C and cooling down to 34 °C, (b) after re-heating up to 400 °C, (c) after holding at 400 °C for 300 s, and (d) after holding at 400 °C for 710 s. All the temperatures were controlled by hot stage heating unit instead of actual values of TEM sample temperature.

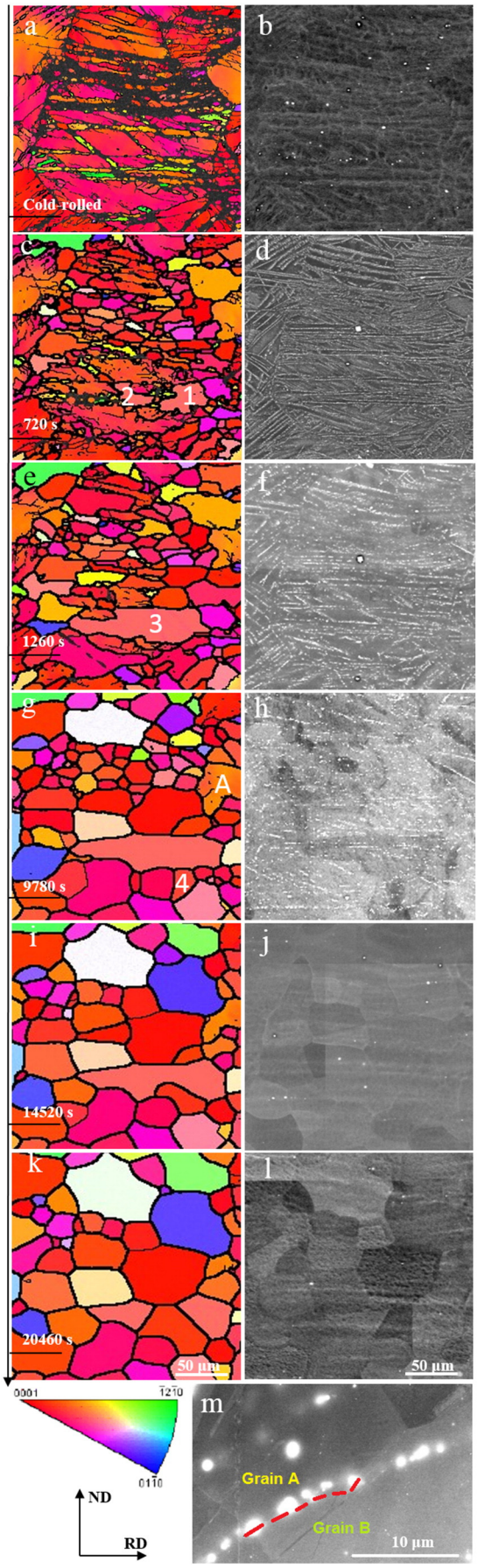

no precipitation was observed in the matrix or within the twins. The entire heating sequence is given in Video 1 with a 4× speed. This clearly demonstrated these precipitates nucleated and grew during isothermal holding at 400 °C, not during cooling. It has not been reported before that precipitates form at such high temperatures, rather, precipitation is normally observed by ageing in the range 100–300 °C to maximise the ageing hardening response [19–22]. Clearly, the current work shows that twin and grain boundaries are preferential sites for precipitation at these high temperatures, Figs. 1-2 and Figs. S2–3.

Another SST10MCR sample was heated to 450 °C and cooled down to 34 °C immediately in the TEM to obtain some precipitation along the boundaries. Subsequently, this sample was re-heated to 400 °C. Fig. S5 plots the re-hearting curve. Fig. 3 provides a series of images showing the dissolution of the precipitates. Fig. 3(a) shows the sample after being heated to 450 °C and cooled down to 34 °C. The precipitates can be clearly seen along the twin and grain boundaries. After re-heating to 400 °C, Fig. 3(b), the size of the precipitates along twin and grain boundaries had increased. However, when the sample was held at 400 °C for a further 300 s, most of the precipitates dissolved, except some larger sized particles, for example, particle A marked in Fig. 3(c). After holding temperature of 400 °C for 710 s, the twin and grain boundaries became clear of second phase particles, except for particle A, which had reduced in size, Fig. 3(d). The entire dissolution process is given in Video 2 with a 4× speed. Thus, nucleation, coarsening and dissolution of precipitates on twin and grain boundaries all occurred at this temperature (Figs. 2-3). It would not be expected that each of these three processes would occur at the same temperature. We propose that the reasons for precipitation at such a high temperature were a result of the combined effects of solute segregation and high local residual strain. Nie [8] and Somekowa [9] reported solute segregated to the twin boundaries. Fig. S6 presents EBSD band contrast and kernel average misorientation (KAM) images of SST1HCR, which shows that there was considerably higher local residual strain in the region of twin boundaries. Segregation on the twin and grain boundaries led to nucleation and growth of the precipitates, which could partly relieve the strain energy. But thereafter, thermodynamically favourable dissolution occurred [23].

To investigate the effect of precipitates on grain growth, it is difficult to use TEM to track the recrystallization and grain growth directly, so the combination of *in-situ* EBSD and *in-situ* SEM were employed to explore how these precipitates affected the growth of recrystallized grains. Fig. 4(a–l) shows the evolution within one grain of sample SST1HCR (same area of Fig. S6) from the deformed structure to full recrystallization annealing at 490 °C for times up to 20,460 s. The left column provides *in-situ* EBSD IPF maps, while the right column gives the corresponding backscattered SEM images. Fig. 4(a) shows an IPF image of one deformed grain after cold rolling, which mainly consisted of double twins $\{10\bar{1}1\}$–$\{10\bar{1}2\}$. Fig. 4(b) shows occasional coarse intermetallic particles, but no precipitates on twin or grain boundaries. After annealing at 490 °C for 720 s, Fig. 4(c) shows nearly all the twins had recrystallized (compare with the non-indexed regions shown in Fig. 4(a)). Growth of the recrystallized grains occurred preferentially along the original TBs direction [12,24]. Interestingly, precipitation occurred along the original position of the TBs and grain boundaries, Fig. 4(d) allowing the original position of these boundaries to be observed after recrystallization. Thus, both recrystallization and precipitation processes existed during annealing at the same temperature of 490 °C. However, it was not possible to absolutely identify which process started first or whether both processes occurred simultaneously during annealing. Nevertheless, the available evidence is that the precipitation before or after the early

Fig. 4. Quasi-in-situ EBSD IPF and corresponding backscattered SEM images of sample SST1HCR: (a-b) as-cold rolled, (c-d) after annealing 720 s, (e-f) after annealing 1260 s, (g-h) after annealing 9780 s, (i-j) after annealing 14520 s, (k-l) after annealing 20460 s at 490 °C and (m) high magnification backscattered SEM image of sample SST1HCR after annealing 1260 s showing precipitates pinning the recrystallized grain boundary (dashed line).

stages of recrystallization did not effectively retard nucleation of recrystallized grains. This was most probably due to the Zenner pinning from the precipitates being too small and the driving force for recrystallization being too high, a result of the substantial local strain around twin sites (as shown in Fig. S6).

The effect of precipitate evolution during annealing on growth of recrystallized grains should be considered. The growth of the recrystallized grains labelled 1 and 2 in Fig. 4(c) were tracked to investigate this effect. After annealing for 1260s, these two grains quickly consumed the deformed area between them and evolved into one larger grain 3 (Fig. 4(e)). As with grains in the upper area, grain 3 expanded preferentially along the original twin boundary direction, even though the original twin boundaries had been consumed by recrystallization. Fig. 4(f) provides the corresponding backscatter SEM image. It shows that most of the precipitates that had formed on the twin boundaries had coarsened. Therefore, particle pinning as well as the solute drag can be considered to be the main mechanisms of restricting grain growth [25]. To further confirm this, Fig. 4(m) gives a high magnification backscatter SEM image of sample SST1HCR after annealing 1260s showing precipitates located along a new recrystallized grain boundary (dashed line).

With further annealing to 9780 s, there was evidence of dissolution of the precipitates, Fig. 4(g,h). All the deformed grains had recrystallized, except area A, Fig. 4(g). The smaller grains exhibited further grain growth and coalescence, while grain 3 did not grow perpendicular to the original TBs direction. After 14,520 s almost all the precipitates had dissolved, Fig. 4(j). Therefore, the solute drag was greater for the GBs with higher solute concentration. Finally, after annealing for 20,460 s, grain 4 consumed grain 3 and split it into two small grains. Considering the whole region in Fig. 4(k), most of the grains were elongated along the initial TBs directions [25].

In summary, this work directly observed precipitation along twin and grain boundaries that later dissolved into the matrix before full recrystallization at 490 °C by using the combination of *in-situ* TEM, *quasi-in-situ* EBSD and SEM methods. Solute segregation and precipitates co-existed along twin and grain boundaries in the early stage of recrystallization. Subsequently, these precipitates coarsened, and although all the twins disappeared the remaining precipitates restricted the grain growth perpendicular to the original twin boundaries. Finally, these precipitates dissolved into the matrix when recrystallization was nearly complete. The solute segregated to grain boundaries exerted strong solute drag along these grain boundaries and restricted their movement during grain growth, which caused unusual grain growth behaviour: the size of recrystallized grains were controlled by the pre-existing twin boundaries. This work observed this unusual phenomenon for the first time: the precipitation occurred along twin boundaries during recrystallization and subsequently dissolved before full recrystallization at an unexpectedly high temperature.

Supplementary data to this article can be found online at http://dx.doi.org/10.1016/j.scriptamat.2017.05.015.

Acknowledgements

This work was funded by the EPSRC DARE Project, EP/L025213/1.

References

[1] L. Priester, Precipitation at Grain Boundaries, Grain Boundaries: From Theory to Engineering, Springer Netherlands, Dordrecht, 2013 217–240.
[2] C. Liu, H. Chen, J.-F. Nie, Scr. Mater. 123 (2016) 5–8.
[3] J.P. Hadorn, T.T. Sasaki, T. Nakata, T. Ohkubo, S. Kamado, K. Hono, Scr. Mater. 93 (2014) 28–31.
[4] J. Robson, Metall. Mater. Trans. A 45 (2014) 3205–3212.
[5] J.D. Robson, S.J. Haigh, B. Davis, D. Griffiths, Metall. Mater. Trans. A 47 (2016) 522–530.
[6] E. Rabkin, Scr. Mater. 42 (2000) 1199–1206.
[7] I. Nikulin, A. Kipelova, S. Malopheyev, R. Kaibyshev, Acta Mater. 60 (2012) 487–497.
[8] J.F. Nie, Y.M. Zhu, J.Z. Liu, X.Y. Fang, Science 340 (2013) 957–960.
[9] H. Somekawa, H. Watanabe, D.A. Basha, A. Singh, T. Inoue, Scr. Mater. 129 (2017) 35–38.
[10] D.A. Basha, R. Sahara, H. Somekawa, J.M. Rosalie, A. Singh, K. Tsuchiya, Scr. Mater. 124 (2016) 169–173.
[11] J. Ye, X.-p. Lin, T.-b. Zhao, N.-n. Liu, H.-b. Xie, Y. Niu, F. Teng, Mater. Sci. Eng. A 663 (2016) 49–55.
[12] D. Griffiths, Mater. Sci. Technol. 31 (2015) 10–24.
[13] Z.R. Zeng, Y.M. Zhu, S.W. Xu, M.Z. Bian, C.H.J. Davies, N. Birbilis, J.F. Nie, Acta Mater. 105 (2016) 479–494.
[14] S.R. Agnew, J.F. Nie, Scr. Mater. 63 (2010) 671–673.
[15] B.-C. Suh, M.-S. Shim, K.S. Shin, N.J. Kim, Scr. Mater. 84–85 (2014) 1–6.
[16] J. Hirsch, T. Al-Samman, Acta Mater. 61 (2013) 818–843.
[17] D. Guan, W.M. Rainforth, L. Ma, B. Wynne, J. Gao, Acta Mater. 126 (2017) 132–144.
[18] M.D. Nave, M.R. Barnett, Scr. Mater. 51 (2004) 881–885.
[19] J.-F. Nie, Metall. Mater. Trans. A 43 (2012) 3891–3939.
[20] J.F. Nie, Scr. Mater. 48 (2003) 981–984.
[21] J.F. Nie, B.C. Muddle, Scr. Mater. 40 (1999) 1089–1094.
[22] J.F. Nie, B.C. Muddle, Acta Mater. 48 (2000) 1691–1703.
[23] H.E. Friedrich, B.L. Mordike, Magnesium Technology: Metallurgy, Design Data Applications, Springer, New York, 2010.
[24] I. Basu, T. Al-Samman, Acta Mater. 96 (2015) 111–132.
[25] F.J. Humphreys, M. Hatherly, Recrystallization and Related Annealing Phenomena, Elsevier Science, 2004.